Journal Pre-proof

TPMS_Scaffold_Generator: A Scaffold-Structure Generator Based on Triply Periodic Minimal Surfaces

Di Lin，Cong Zhang，Xiyong Chen，Nannan Wang，Lei Yang

Please cite this article as: Di Lin， Cong Zhang， Xiyong Chen， Nannan Wang， Lei Yang， TPMS_Scaffold_Generator: A Scaffold-Structure Generator Based on Triply Periodic Minimal Surfaces, *Additive Manufacturing Frontiers* (2024), doi: https://doi.org/10.1016/j.amf.2024.200123

This is a PDF file of an article that has undergone enhancements after acceptance, such as the addition of a cover page and metadata, and formatting for readability, but it is not yet the definitive version of record. This version will undergo additional copyediting, typesetting and review before it is published in its final form, but we are providing this version to give early visibility of the article. Please note that, during the production process, errors may be discovered which could affect the content, and all legal disclaimers that apply to the journal pertain.

Highlights:

- TPMS scaffold generator offers functions of generating TPMS-based scaffold architectures

- The pinch-off problem of TPMS-based scaffold can be solved efficiently to some extent.

- Shell-based scaffold and skeleton-based scaffold with low volume fraction can be generated

- The mechanical properties of scaffold can be adjusted by varying relating variables

- Heterogeneous scaffold with gradient in cell size, volume fraction, topology type can be created

1

TPMS_Scaffold_Generator: A Scaffold-Structure Generator Based on Triply Periodic Minimal Surfaces

Di Lin [a], Cong Zhang [a,*], Xiyong Chen [b], Nannan Wang [b], and Lei Yang [a, c,*]

[a] School of Transportation and Logistics Engineering, Wuhan University of Technology, Wuhan, China

[b] MOE Key Laboratory of New Processing Technology for Non-ferrous Metals and Materials, Guangxi Key Laboratory of Processing for Non-ferrous Metals and Featured Materials, Guangxi University, Nanning, China

[c] State Key Laboratory of Materials Processing and Die & Mould Technology, School of Materials Science and Engineering, Huazhong University of Science and Technology, Wuhan, China

Abstract: With the rapid development of additive manufacturing (AM), scaffold architectures based on triply periodic minimal surfaces (TPMS) have attracted increasing interest in various engineering fields. Nevertheless, they are limited because of the complexity of the design process when adopted in different research and engineering fields. In this work, we present a free and easy-to-use software package called TPMS_Scaffold_Generator, which is coded using MATLAB (Mathworks, Inc., USA). It offers three function tabs which are homogeneous tab, heterogeneous tab and multisymmetrical tab, respectively. Variables of the tabs include including the volume fraction, topology type, unit cell size, the length of architecture in *X*, *Y*, *Z* direction, accuracy, and the style of gradient and so forth. TPMS_Scaffold_Generator can generate various TPMS scaffolds, especially ultralight and multisymmetrical scaffolds. The latest version of the TPMS_Scaffold_Generator is freely available at: https://github.com/LeveeLin/TPMS_Scaffold_Generator.git.

Keywords: TPMS scaffold generator; Ultra-light scaffolds; Triply periodic minimal surfaces (TPMS); Multisymmetrical scaffolds

Corresponding authors: lei.yang@whut.edu.cn(L. Yang); zhangcong@whut.edu.cn(C. Zhang)

1. Introduction

Cellular materials have been widely investigated for their superior properties, such as light weight, load bearing, damping, strain isolation, energy absorption, crack arresting, and self-healing [1]. The representative cellular materials, cellular solids, such as cork, wood, sponge, and trabecular

bone, are composed of an interconnected array of struts or sheets. Their architecture can be obtained through either open- or closed-cell types connected in an orderly, periodic, or stochastic manner [2].

In addition, honeycombs [3] and foam [4] are engineering cellular solids that have been commonly used over the past two decades. The honeycomb cellular architecture, which can be designed as a two-dimensional template and extruded in a third direction, originates from honeycombs in nature. Unlike honeycombs, foam is a three-dimensional cellular material that contains complex cell geometries [5]. However, their widespread adoption is hindered by unavoidable process-related defects, the restricted control over foam's morphology, and the honeycomb's simplex two-dimensional architecture. With the development of additive manufacturing, triply periodic minimal surface (TPMS) scaffolds offer useful methods to solve these problems [6].

TPMS-based scaffolds are useful in many engineering applications and industries, such as construction [7, 8], electrical [9], acoustic [10], transportation [11-13], chemical [14], optical [15] and energy [16]. The surfaces of such architectures are smooth, without edges or corners. This feature decreases the stress concentration observed in typical lattice network structures [17]. In addition, TPMS-based porous scaffolds have a wide range of fascinating topological features, such as bioinspired morphology, length scales, and structurally controlled characteristics. Therefore, these scaffolds exhibit excellent characteristics, including a high stiffness-to-weight ratio, heat-dissipation control, and enhanced mechanical-energy absorption [18]. Geometric features, such as the cell size, topology, and volume fraction [19] are the main factors controlling the mechanical and physical properties of these cellular materials [20].

Moreover, in additive manufacturing (AM), TPMS-based scaffolds can offer lightweight yet strong interior support to the boundary of a printed model. TPMS-based porous scaffolds can be further classified as skeleton-based and shell-based. As a result, a number of variables, including the scaffold type, unit-cell topology type, unit-cell size, and percent porosity, can be used to design a scaffold that meets different engineering requirements. Relevant software must be designed to better investigate the mechanical and physical properties of TPMS-based scaffolds.

On the one hand, as a consequence of the outstanding performance of TPMS-based scaffolds, a number of computer-aided-design (CAD) programs have been developed for scaffold-architecture generation. Many powerful commercial software packages exist , such as the Autodesk Netfabb software [21], Materialise 3-matic, the Materialise Magics Structures Module [22], and nTopology [23]. They feature lattice generation and provide considerable freedom in lattice design. However, they are so expensive that researchers have difficulty investigating the relationship between the geometric parameters and properties of TPMS-based scaffolds.

On the other hand, Autodesk provides a free software package called Meshmixer [24], which provides limited lattice-design abilities that help with AM build preparation, stereolithography (STL) file repair, orientation optimization, support generation, etc. [25]. Some helpful and free software packages are also available, including the MATLAB-based STL Lattice Generator [26], Minisurf [27], FLatt Pack [25] and MSlattice [28].

Among them, the Lattice Generator and Minisurf are open source, which greatly helps researchers to study the principles of generating TPMSs and their scaffolds. Unfortunately, they both have minimal functionality, which makes it difficult for researchers to further investigate the structure–property relationships.

Both FLatt Pack and MSlattice are powerful software packages with good scaffold visualization and optional variables, such as cell size, topology type, and scaffold volume fraction. Although MSlattice offers flexibility in allowing users to design their own TPMS lattice, based on level-set approximations, it is difficult for users to build a hybrid of two different scaffolds because of the difficulties in finding suitable level-set approximations and adjusting variables. Hence, a simple, easy-to-use, and affordable software package for designing and generating TPMS-based scaffolds is still lacking.

To better understand the material–topology–property relationship that can be used to control the functionality of a scaffold architecture or component, we propose TPMS_Scaffold_Generator. It offers many options for significant variables. Using this software, users can adjust the scaffold type, unit-cell topology type, unit-cell size, percent porosity, and accuracy. In addition, because AM provides access to scaffold architectures, TPMS_Scaffold_Generator offers homogeneous and heterogeneous tabs. Users can generate a uniform TPMS-based scaffold using the homogeneous tab. In the heterogeneous tab, users can generate graded scaffolds whose gradients can be in the volume fraction, cell size, or heterostructure.

In this study, we describe TPMS_Scaffold_Generator. TPMSs are introduced in Section 2.1 because they are significant structures for designing functional porous scaffold architectures, owing to the advent of additive-manufacturing techniques [29]. Functionally graded TPMS structures are characterized by various structures and mechanical properties, thereby presenting better mechanical properties than homogeneous structures. Gradient strategies for the volume fraction, cell size, and cell-topology type are introduced in Section 2.3.

2. Methodology

## 2.1. Triply periodic minimal surfaces

Generally, a minimal surface is defined as a surface in which the mean curvatures vanish at every point. A minimal surface that is infinite and periodic in three independent directions is called a triply periodic minimal surface (TPMS) [18]. A surface is a set of points with a constant function value. A zero-valued surface, known as a zero or level set, represents the interface regions of the space lying on, inside, or outside the space [30].

TPMS_Scaffold_Generator has eight built-in TPMSs, including the primitive (P) and diamond (D) surfaces discovered by Schwarz [31], and the gyroid (G), I-graph and wrapped package-graph (IWP), face-centered cubic rhombic dodecahedron (FRD), Neovius (N), Fischer–Koch (F), and lidinoid (L) surfaces [32]. They can be approximated by the level-set surfaces of trigonometric functions [33-35] listed in Table 1.

Table 1. Eight types of level-set surfaces of trigonometric functions.

Styles	Trigonometric equations
U_P	$\cos X + \cos Y + \cos Z - t = 0$
U_D	$\sin X \sin Y \sin Z + \sin X \cos Y \cos Z + \cos X \sin Y \cos Z + \cos X \cos Y \sin Z - t = 0$
U_G	$\sin X \cos Y + \sin Y \cos Z + \sin Z \cos X - t = 0$
U_{IWP}	$2(\cos X \cos Y + \cos Y \cos Z + \cos Z \cos X) - (\cos X + \cos Y + \cos Z) - t = 0$
U_{FRD}	$8(\cos X \cos Y \cos Z + \cos 2X \cos 2Y \cos 2Z) -$ $(\cos 2X \cos 2Y + \cos 2Y \cos 2Z + \cos 2Z \cos 2X) - t = 0$
U_N	$3(\cos X + \cos Y + \cos Z) + 4(\cos X \cos Y \cos Z) - t = 0$
U_F	$\cos 2X \sin Y \cos Z + \cos 2Y \sin Z \cos X + \cos 2Z \sin X \cos Y - t = 0$
U_L	$0.5(\sin 2X \cos Y \sin Z + \sin 2Y \cos Z \sin X + \sin 2Z \cos X \sin Y) -$ $0.5(\cos 2X \cos 2Y + \cos 2Y \cos 2Z + \cos 2Z \cos 2X) + 0.15 - t = 0$

In these equations, X, Y, and Z refer to $2\pi x/a$, $2\pi y/a$, and $2\pi z/a$, respectively. Moreover, the constant t controls the volume surrounded by the cell surface, as well as the position of the boundary between two subdomains [36]. Parameter a is the unit-cell size [32, 37]. As shown in Fig. 1, eight TPMSs were generated using MATLAB (Mathworks, Inc., USA).
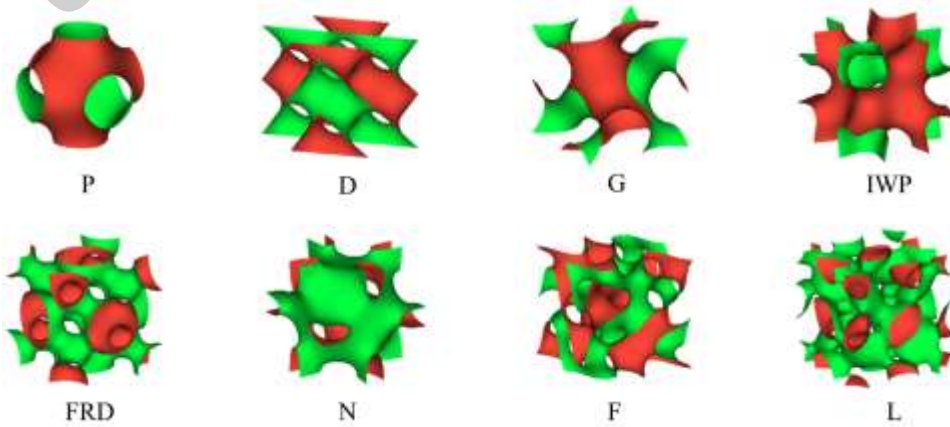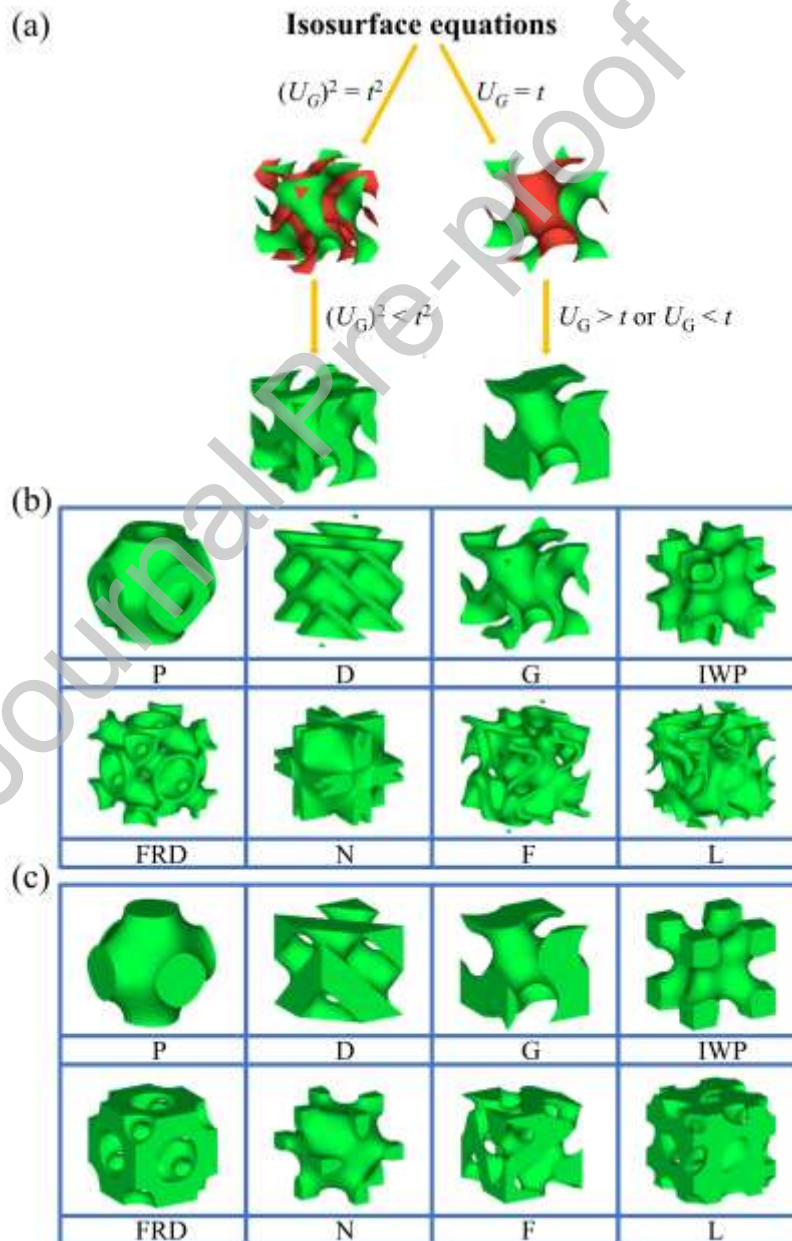

Fig. 1. Eight TPMSs, in which each unit cell is 1 mm × 1 mm × 1 mm and $t = 0$.

5

2.2. Design of uniform scaffold structures

TPMS-based scaffolds can be classified into two main types, as shown in Fig. 2: skeleton- and shell-based scaffolds [38]. Hence, two methods have been reported for generating TPMS-based structures. These methods rely on determining the isosurface (a surface that follows a constant value within a three-dimensional function) using the marching-cubes algorithm [39].

The first strategy yields shell-based scaffold architectures by thickening the minimal surface, where the thickness is continuous and fixed throughout the surface, as shown in Fig. 2(a). The other strategy produces skeleton-based scaffold structures by solidifying the volumes enclosed by the TPMSs [40, 41]. The methods for creating these two types of scaffolds will be introduced in Sections 2.2.1 and 2.2.2.

Fig. 2. (a) Illustration of the generation of shell-based and skeleton-based scaffolds; (b) Eight unit-cell types of shell-based scaffolds, in which each unit cell is 1 mm × 1 mm × 1 mm and the volume fraction is 30%; (c) Eight unit-cell types of one skeleton-based scaffold in which each unit cell is 1 mm × 1 mm × 1 mm and $t = 0$.

2.2.1. Design of shell-based scaffold structures

As introduced above, we can provide the TPMS with an exact thickness by defining the expression $-t < U < t$ to mathematically create shell-based scaffold architectures. In this study, as shown in Fig. 2(b), eight types of shell-based scaffolds were built using TPMS_Scaffold_Generator. The scaffold structures' volume fraction φ, defined as the ratio of the architectures' volume to the space cubic volume, is related to the value of t (The Materialise Magics software package can show the volume after repairing a model.) This relationship can be determined by function fitting both parameters.

Because the volume fraction is an input parameter of the software, φ is set as an independent variable, while t is set as a dependent variable. According to this method, the scatter plots, fitting equations, and ranges of different styles of volume fractions are presented in Supporting Information 1. Because shell-based architectures have an exact thickness, pinch-off problems do not exist. When the t value is outside the range listed in Supporting Information Part 1, the generated scaffold will be distorted or far from the expected shape. That is, the expected model can only be obtained for a given volume-fraction range.

2.2.2. Design of skeleton-based scaffold structures

A TPMS can partition a symmetrical space into two subdomains. One of them is solidified by mathematically determining $U > t$ or $U < t$ to obtain skeleton-based scaffold structures; the other is a void district. As shown in Fig. 2(c), the generator was utilized to produce eight types of skeleton-based scaffold architectures [18]. Because the volume fraction of the scaffold structures is controlled by the offset value t, both variables can be function-fitted to determine their relationship. The relationship between the value of t and the volume fraction of the scaffolds was specifically investigated, and the details are presented in Supporting Information Part 2.

2.3. Generation of functionally-graded porous scaffolds

The proposed generator can grade the volume fraction, unit-cell size, and multi-morphology (of hybrid scaffolds) of skeleton- and shell-based scaffolds. Porous scaffolds, functionally graded in terms of cell size, are gaining increasing attention in the field of tissue engineering because the cell size varies in diverse places within biological skeletons. Compared with homogeneous architectures, scaffolds with graded cell sizes have better cell adhesion and growth on the bones.

7

2.3.1. Volume-fraction grading

As mentioned above, the volume fraction of TPMS-based scaffold architectures can be controlled by adjusting parameter *t* in the TPMS functions. The constant value *t* in the TPMS functions is replaced with *t*(*x*, *y*, *z*) to enable variations in the volume fraction throughout the scaffold architecture. According to these methods, two types of volume-fraction grading, linear and cosine, are introduced in Supporting Information Part 3.

2.3.2. Unit-cell size gradient

The designed software offers a linear gradient of cell-sized graded scaffolds. U_P is used as an example to show how the related gradient in cell-size graded scaffolds is generated. The corresponding equation is replaced with U_P:

$$\cos(\alpha X) + \cos(\beta Y) + \cos(\gamma Z) - t = 0. \tag{1}$$

The related parameters of Eq. (1) are identical to those of the level-set surfaces of trigonometric functions introduced in Section 2.1, whereas α, β, and γ are important variables that control the unit-cell size.

A comparison of the equations for U_P in Table 1 and Eq. (1) reveals that $\alpha = \beta = \gamma = 1 / a$ for uniform scaffolds. To obtain a linear gradient in cell-size graded scaffolds, *a* can be converted into a linear function, which also means the gradient can be created by defining α, β, and γ as a function about *x*, *y*, and *z*. After applying this method, we obtained a linear gradient in the cell-sized graded scaffolds; the details are presented in Supporting Information Part 4.

2.3.3. Multi-morphologically porous-scaffold design

Natural tissues with different forms cannot be represented by a homogeneous architecture; instead, most of them are multi-morphologically porous scaffolds [42]. Two CAD strategies combine different TPMS-based structures with the given transition boundaries. One is the sigmoid-function (SF) method [43, 44] which can be effectively employed in ordinary transition-frontier cases. The other is the beta growth function (BGF) method, which can easily and accurately hybridize two distinct TPMS porous morphologies [45, 46]. The proposed software employs the SF method. The main content of this method is presented in Supporting Information Part 5.

3. Fabrication and Results

After applying the mathematical expressions introduced in Section 2 to generate TPMS-based architectures using MATLAB (Mathworks, Inc., USA) software, the TPMS_Scaffold_Generator was

written; it can be obtained from https://github.com/LeveeLin/TPMS_Scaffold_Generator.git. The performance of this software is demonstrated in Supporting Information Part 6, and a 3D printed version of the model exported by TPMS_Scaffold_Generator is shown in Supporting Information Part 7.

To further demonstrate the practicability of this software, grade Fischer–Koch scaffolds were created and their mechanical properties were investigated.

3.1 Materials and fabrication process

The Ti_6Al_4V powder used in this study was produced using electrode-induction melting-gas atomization technology (Avimetal Powder Metallurgy Technology Co., Ltd., Beijing, China). A Quanta 650 field-emission gun (FEG) scanning electron microscope (SEM) (FEI, USA) was used to observe the morphology of the Ti_6Al_4V powder. As shown in Fig. 3(a), the Ti_6Al_4V particles were spherical or near-spherical with smooth surfaces. The particle-size distribution of the Ti_6Al_4V powder was measured using a Mastersizer-3000 laser particle-size analyzer (Malvern, England). The size of the Ti_6Al_4V particles ranged from 23.8 μm to 58.8 μm with an average size of 37.7 μm, as illustrated in Fig. 3(b).
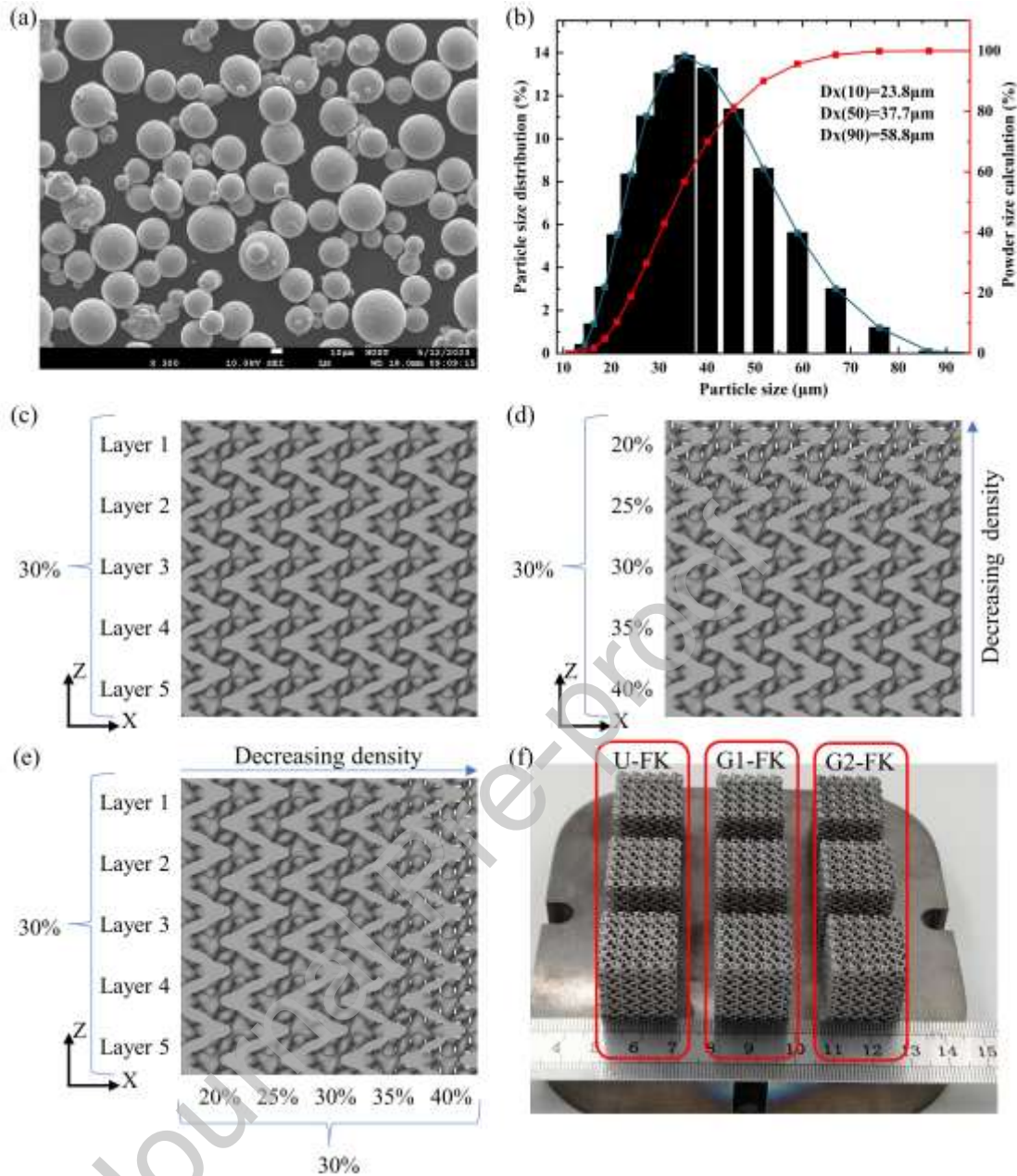
Fig. 3. (a) SEM image; (b) Particle-size distribution of Ti$_6$Al$_4$V powder; (c) 20 mm × 20 mm × 20 mm uniform Fischer–Koch scaffold with 4-mm unit-cell size; (d) 20 mm × 20 mm × 20 mm Z-oriented gradient Fischer–Koch scaffold with 4-mm unit-cell size; (e) 20 mm × 20 mm × 20 mm X-oriented gradient Fischer–Koch scaffold with 4-mm unit-cell size; (f) Photo of the L-PBF-fabricated Ti$_6$Al$_4$V Fischer–Koch TPMS scaffolds.

As shown in Figs. 3(c), (d), and (e), TPMS_Scaffold_Generator was used to create a uniform Fischer–Koch scaffold (U-FK), gradient Fischer–Koch scaffold along the *Z* axis (G1-FK), and gradient Fischer–Koch scaffold along the X axis (G2-FK). The Ti$_6$Al$_4$V Fischer–Koch TPMS scaffolds were fabricated using a commercial DiMetal-100H laser powder-bed fusion (L-PBF) machine (Guangzhou Laseradd Additive Technology Co., Ltd., Guangzhou, China) equipped with a

10

500 W ytterbium fiber laser. Its maximum scanning rate and minimum spot were 7.8 m/s and 20 μm, respectively.

The scaffolds were printed in a high-purity argon atmosphere, and the oxygen content in the building chamber was maintained below 300 ppm. Based on our ongoing experiments, we selected the L-PBF parameters listed in Table 2. The finished Ti_6Al_4V specimens were removed from the substrate using a Mo filament cutter and cleaned using an ultrasonic cleaner with absolute ethyl alcohol.

Fig. 3(f) presents general views of the samples fabricated using L-PBF. No broken struts or cells were observed in the as-prepared samples. This indicates that the Ti_6Al_4V Fischer–Koch TPMS scaffolds were well fabricated using the L-PBF parameters provided in Table 2.

Table 2. L-PBF parameters.

Parameter	Value
Laser power (W)	170
Scanning velocity (mm/s)	1100
Layer thickness (μm)	30
Hatch spacing (μm)	70
Hatch angle (°)	90
Volumetric energy density (J/mm^3)	73.59

3.2 Measurements and characterization

The relative density (RD) of the solid struts of the Ti_6Al_4V Fischer–Koch TPMS scaffolds manufactured by L-PBF is defined as the ratio of the actual density to the theoretical density (4.45 g/cm^3). The actual densities of the scaffolds fabricated by L-PBF were determined using the Archimedes method via a ME204 electronic balance with a 0.1 mg scale increment (Mettler Toledo, Switzerland).

The percentage deviation of the volume fraction between the Ti_6Al_4V Fischer–Koch TPMS scaffold fabricated by L-PBF and the designed CAD model was defined as the ratio of the difference between the actual and designed volume fractions to the designed volume fraction. The actual relative densities of the samples were obtained by dividing the actual volume of the solid struts of the as-built specimens by the total volume of the cubic samples. The actual volume of the solid struts was measured using the Archimedes method. The total volume of the cubic sample was calculated according to its overall dimensions, which were determined using a digital Vernier caliper with a 0.01 mm increment (Greener, China). Table 3 shows the measured dimensions, weights, and densities of the fabricated Fischer–Koch samples.

The mechanical behaviors of the Ti_6Al_4V Fischer–Koch TPMS scaffolds were investigated through uniaxial compression tests at room temperature (RT) along the building direction (*Z*-axis) at

a 0.02 mm/s strain using an AG-IC 100 KN electronic universal-testing machine (Shimadzu, Japan). The applied loads were obtained to calculate the compressive stress by dividing the value of the load by the effective area of the scaffold structure. The strain was calculated by dividing the displacement of the upper compression die by the original height of the Ti_6Al_4V Fischer–Koch TPMS scaffold.

Table 3. Dimensions, weights, and densities of the fabricated Fischer–Koch samples.

Designed Scaffold	Actual dimensions of cellular cubic $X \times Y \times Z$(mm)	Weight (g)	RD of Solid struts (%)	Actual RD ρ (%)	Mean RD $\bar{\rho}$ (%)	Deviation ηRD (%)
U-FK (1)	20.23×20.20×20.18	12.32	98.1	33.87		
U-FK (2)	20.16×20.16×20.21	12.32	98.0	33.99	33.93	13.10
G1-FK (1)	20.15×20.16×20.19	12.38	98.1	34.18		
G1-FK (2)	20.17×20.16×20.17	12.29	98.2	33.86	34.02	13.41
G2-FK (1)	20.18×20.16×20.17	12.26	98.0	33.88		
G2-FK (2)	20.16×20.16×20.14	12.31	98.0	34.12	34.00	13.33

3.3 Deformation and collapse stages of the Fischer–Koch scaffolds

Fig. 4 shows the deformation stages recorded by a high-speed camera for U-FK, G1-FK, and G2-FK at strain levels of 0%, 20%, 25%, 35%, and 45%. Fig. 5 illustrates the experimental stress–strain curves of the Fischer–Koch scaffolds under a uniaxial compression test.

As shown in Fig. 4, for U-FK and G1-FK, the initial cracks (indicated by white circles) appeared in the first layer. It is noticeable that the crack in G1-FK initiated at a strain of only 4%, owing to the lower density in the first layer than that of U-FK. In addition, most cracks appeared in relatively thin structs.

With increasing compressive strain, both holistic structures exhibited layer-by-layer collapses. For G2-FK, the initial crack appeared at a strain of 7%, which was the same as its counterpart U-FK. This is because the densities of these two structures in each layer along the *Z* axis are identical. However, the fracture phenomena differ. U-FK shows a layer-by-layer collapse, whereas G2-FK has a nearly 45° fracture band. This is because the volume fraction of G2-FK along the *X*-axis changes in the *X-Y* plane.

As shown in Fig. 5, although the overall mechanical properties of the three types of samples are different, they exhibit similar four-stage mechanical responses. In the first stage, known as the elastic-deformation stage, the stress increases linearly with increasing strain, and the slope represents the compressive modulus.

The second stage is a linear–plastic deformation stage in which the stress–strain curve leaves the linear response. The nominal yield strength is determined by the stress at which the stress–strain curve for axial loading deviates by 0.2% from the linear-elastic region. In this linear–plastic deformation stage, the stress increases nonlinearly with an increase in the compression strain until it

reaches the maximum stress, denoted as the ultimate strength. Subsequently, a noticeable decline in stress is observed in the stress–strain curve after a short yield plateau.

The stress–strain curve then enters the third stage, which is a long plateau region with fluctuating stress. Finally, a large number of structs in these structures are destroyed and squeezed together, and the stress–strain curve becomes denser, in which the stress increases as the strain rises.

In addition, it is clear from Fig. 5 that the deformation responses of U-FK and G2-FK are very similar, which is identical to the strain at which their initial cracks appear. This is because the density of each layer in both structures is uniform (30%). Nevertheless, the deformation response of G1-FK differs from those of the other two. Its ultimate strength is obviously lower than those of U-FK and G2-FK, mainly because the density of its first layer is relatively low, at 22%.
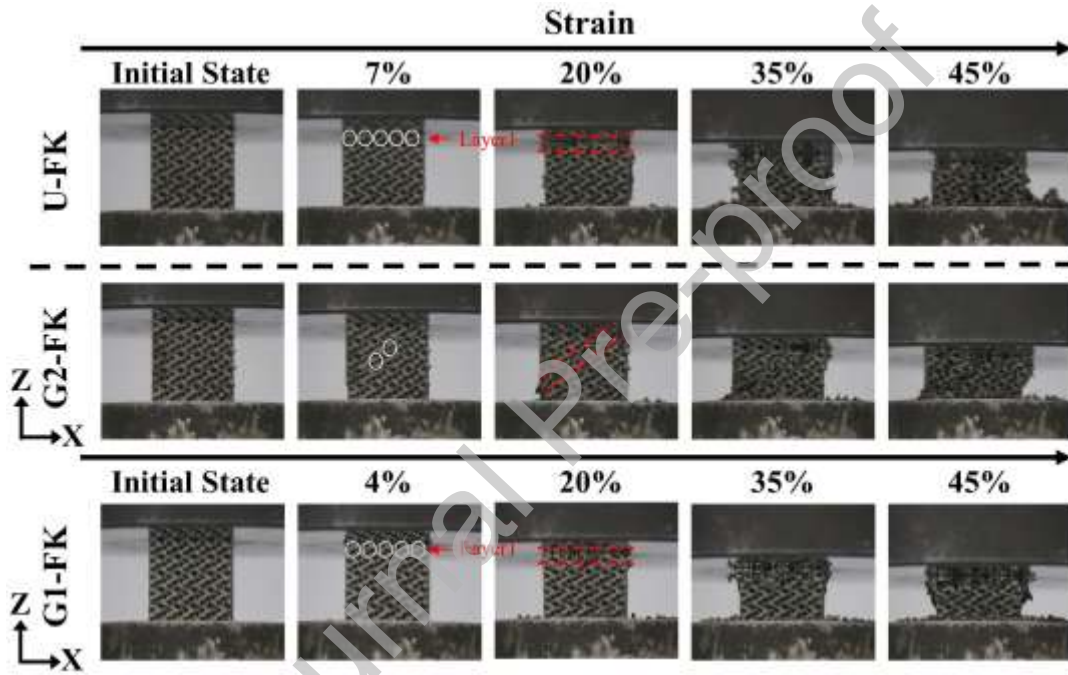
Fig. 4. Footage captured during uniaxial compression at different strain stages for three types of Fischer–Koch scaffolds.
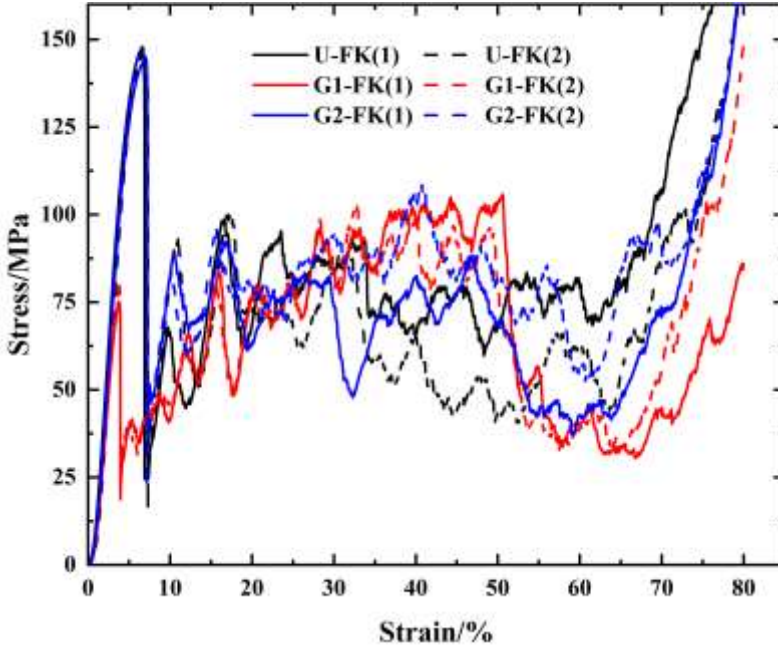
Fig. 5. Compressive stress–strain curves of Fischer–Koch scaffolds.

4. Discussion

4.1 Relationship between the accuracy and volume fraction

The obtained TPMS scaffold is highly dependent on the accuracy-controlling parameter, which is the number of mesh points in a unit.

The accuracy-controlling parameter is denoted by A in Fig. 6 and 7 is related to the volume fraction of the scaffold when the pinch-off problem is investigated. When this software was used to create a skeleton-based IWP scaffold with a 1% volume fraction, the scaffold was discontinuous. However, this can be resolved by adjusting the accuracy to 100 or more. Therefore, we chose three groups of scaffolds with a wide range of accuracy values, as shown in Fig. 6.

Clearly, when the accuracy is too low, a discontinuity or pinch-off problem appears. For example, primitive scaffolds with $A = 7.9$, gyroid scaffolds with $A = 15$ and 20, and IWP scaffolds with $A = 15, 20, 30,$ and 50 are discontinuous. In addition, the volume fraction of these scaffolds is lower than anticipated (here, 1%). The volume fraction of scaffolds with high accuracy will increase subtly, with few effects on our anticipated targets. In conclusion, users can input a higher accuracy value to solve the discontinuity and obtain scaffolds with a low volume fraction.

14
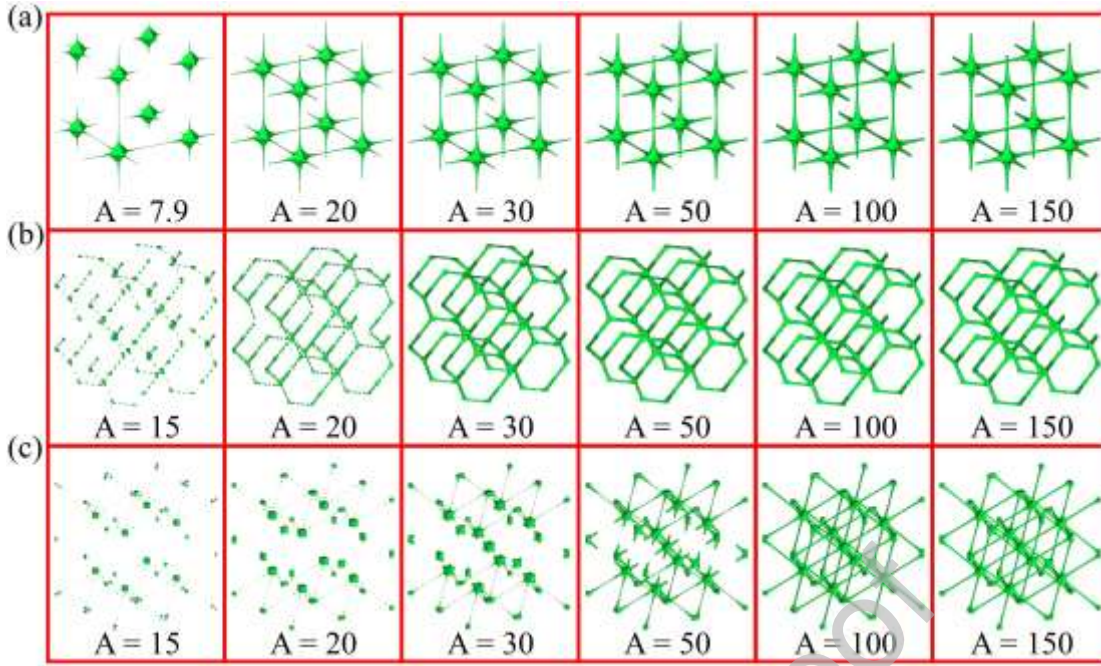
Fig. 6. Skeleton-based scaffolds whose volume fraction is set to 1%: (a) Primitive scaffolds; (b) Gyroid scaffolds; (c) IWP scaffolds.

It is also necessary to investigate the relationship between the accuracy and scaffolds with higher volume fractions; the related data are shown in Fig. 7. We can see from the chart that a higher accuracy has little effect on the volume fraction of the scaffolds; therefore, this phenomenon can be ignored.
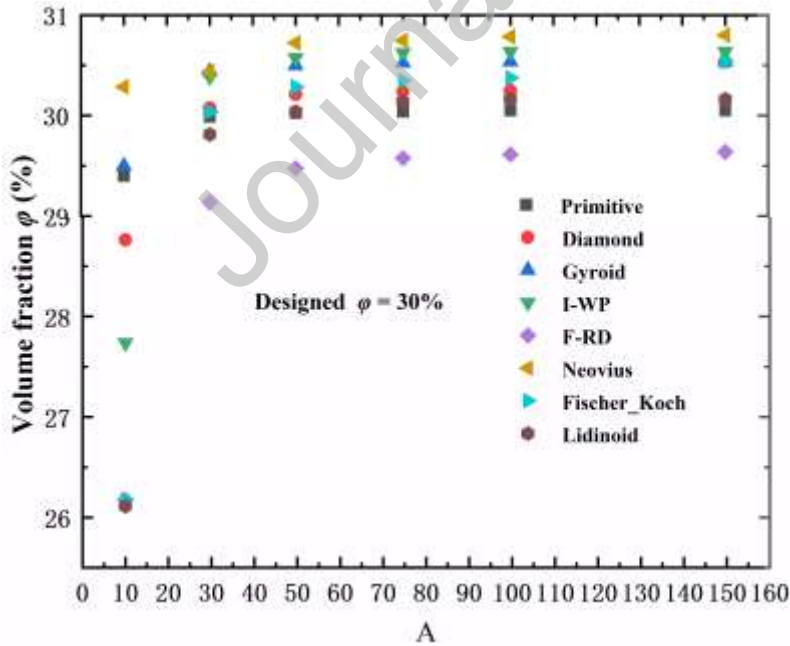
Fig. 7. Actual volume fraction of skeleton-based scaffolds with input parameter (volume fraction = 30%).

When the accuracy is too low, two problems occur. First, the connections of the triangular patches are not sufficiently smooth because of the lower accuracy. Hence, the volume fraction of the scaffolds, including the primitive, diamond, gyroid and I-WP, will be slightly lower than expected.

Secondly, a pinch-off problem occurs. For example, the volume fractions of F-RD, Fischer–Koch, and lidinoid (26.175%, 26.175%, and 26.1125%, respectively) were significantly lower than 30%. In other words, the scaffold becomes discontinuous when the accuracy is low, and the volume fraction of the scaffold appears to be lower than expected.

4.2. Complicated TPMS scaffolds

4.2.1. Multi-dimensional TPMS scaffolds

In addition to the functional method mentioned in Section 2.3.1, interpolation can be used to generate scaffolds with a linear gradient. In Fig. 8, linear-gradient IWP structures are used to demonstrate the results of the interpolation method. This method can flexibly generate multiple linear gradients within a structure, although many interpolation points must be provided so that ideal models can be obtained; this is inconvenient when using input statistics.

In addition, this strategy is useful for obtaining scaffolds with two-dimensional and three-dimensional gradients. First, 2D-Gyroid1 (G1), 2D-Gyroid2 (G2), and 2D-Gyroid3 (G3) are used to show the generated situations. The interpolation of G1 and G2 is in accordance with a certain law; therefore, an ideal outcome is obtained, as shown in Fig. 9. However, when the volume fraction of the G3 interpolation has no rules, the alteration in the volume fraction is not easily controlled. This problem can be resolved by adding more interpolation points to each dimension. The IWP was selected as the 3D-gradient model to demonstrate the generation of 3D complex structures using the interpolation method, as shown in Fig. 10.
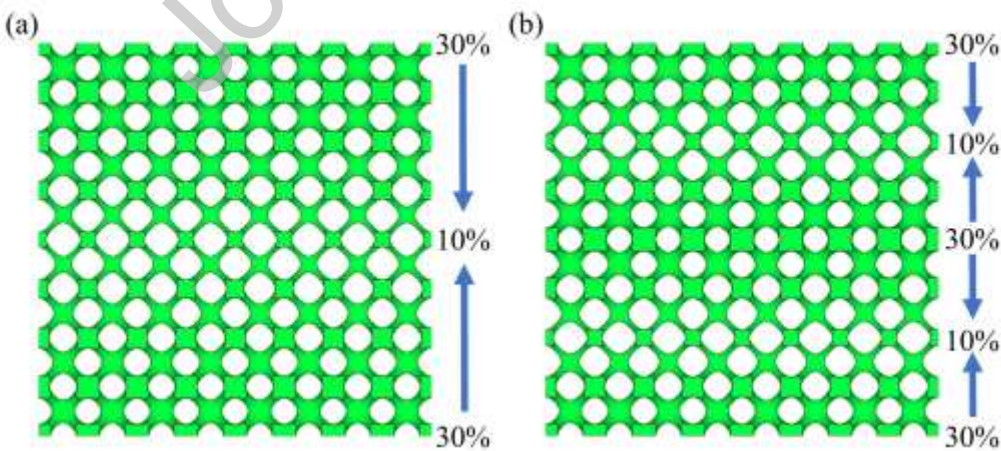
Fig. 8. IWP scaffolds with a linear gradient generated using the interpolation method: (a) IWP structure with two linear gradients; (b) IWP structure with four linear gradients.
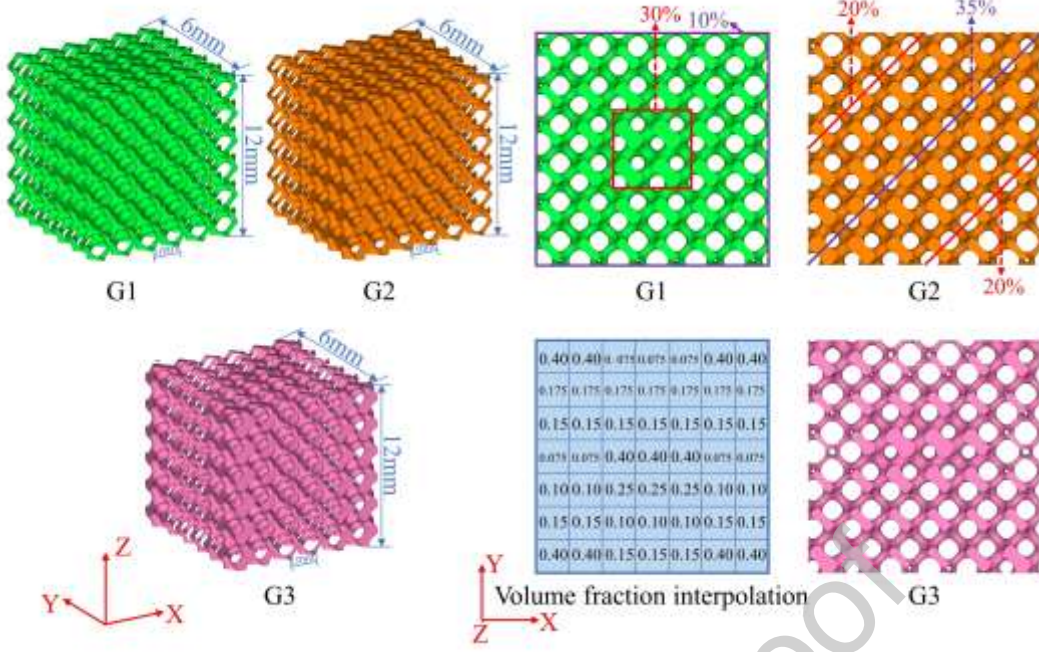
Fig. 9. Stereo plots and top views of G1, G2, and G3.
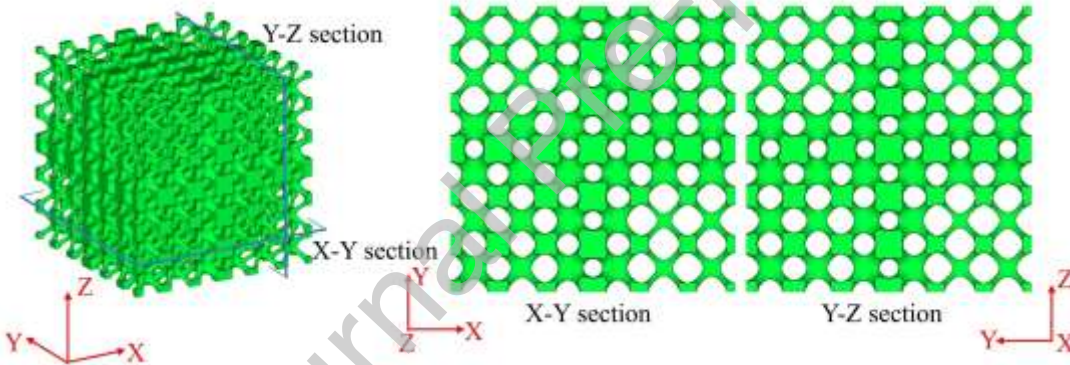

Fig. 10. 3D-IWP scaffold.

4.2.2. Multisymmetrical TPMS scaffolds

Inspired by the polycrystal-based architectural materials proposed by Chen et al. [47-49], we created a new function for TPMS_Scaffold_Generator that enables it to provide STL files of diagonally symmetrical and four-fold symmetrical TPMS scaffolds. Gyroid scaffolds will be used as examples of the design of multisymmetrical TPMS scaffolds. All of them are 20 mm × 20 mm × 20 mm, with a 5-mm unit-cell size and 10% volume fraction.
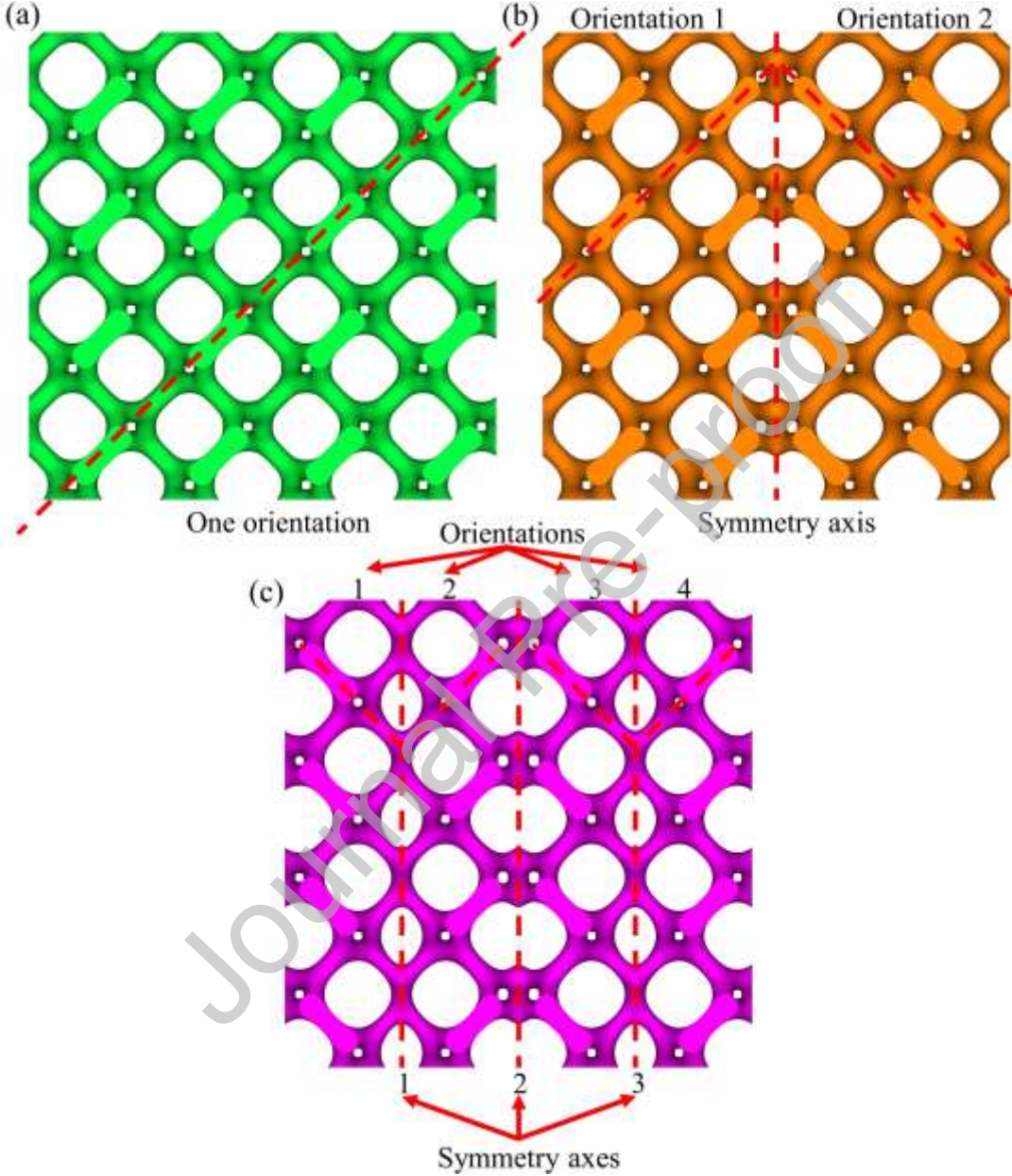
4.2.2.1 Diagonally symmetrical TPMS scaffolds

As mentioned above, the diagonally symmetrical gyroid scaffold can be divided into two sections: one controlled by $U_G (x, y, z)$ and the other described by $U_G (-x, y, z)$. To smooth the

17

transition of the boundary or symmetry axis, the SF method described in Supporting Information 5 is introduced. Therefore, the diagonally symmetrical gyroid scaffold can be expressed as:

$$U_{two\text{-}sym}(x, y, z) = \mu(x, y, z) \, U_G(x, y, z) + (1- \mu(x, y, z)) \, U_G(-x, y, z). \qquad (2)$$

As shown in Fig. 11(b), the generated diagonally symmetrical gyroid scaffold has two orientations, compared to the uniform gyroid scaffold shown in Fig. 11(a).

Fig. 11. (a) Uniform gyroid TPMS scaffold; (b) Two-fold symmetrical gyroid scaffold with two orientations; (c) Four-fold gyroid scaffold with four orientations

4.2.2.2 Four-fold symmetrical TPMS scaffolds

Building on the diagonally symmetrical TPMS scaffolds, four-fold symmetrical TPMS scaffolds can be created using the following expression:

$$U_{four\text{-}sym}\,(x,\,y,\,z) = \mu\,(x,\,y,\,z)\,U_{two\text{-}sym}\,(x,\,y,\,z) + (1 - \mu\,(x,\,y,\,z))\,U_{two\text{-}sym}\,(-x,\,y,\,z). \,(3)$$

As illustrated in Fig. 11(c), this scaffold has four orientations and three symmetry axes compared with the uniform scaffold.

The method of generating multi-symmetrical scaffolds using TPMS_Scaffold_Generator is detailed in Supporting Information Part 6.

4.3 Scaffolds with different shapes

Scaffolds with different shapes can be easily obtained through Boolean operations in software, such as Materialise Magics. TPMS_Scaffold_Generator offers TPMS-based materials to conduct a Boolean operation so that an ideal scaffold can be obtained. The Boolean operation process is illustrated in Fig. 12.

Object   TPMS material   Target
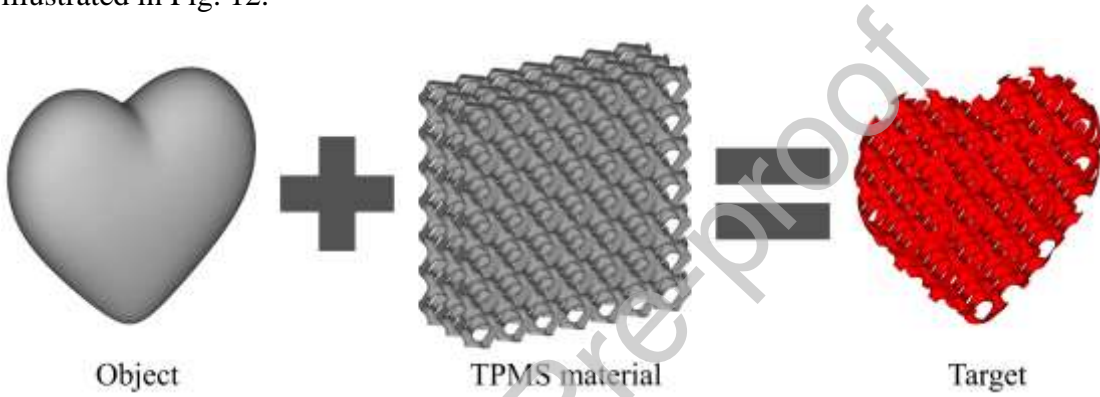
Fig. 12. 3D object infilled with TPMS material.

4.4 Transitions between two different scaffolds

In Supporting Information Part 5, an example of the transition shape is only a large plane whose expression is $Z = C$. We know that the transition shape can be changed through $G(x, y, z)$ from Eq. (S13). As shown in Fig. 13, cylindrical and spherical shapes were used to generate 6 mm × 6 mm × 6 mm multi-morphology scaffolds. In addition, plane transitions can occur along different orientations, as shown in Fig. 13(c).

Cylinder: $G_1(x, y, z) = x^2 + y^2 - R^2$;

Sphere: $G_2(x, y, z) = x^2 + y^2 + z^2 - R^2$;

Plane: $G_2(x, y, z) = y - C$.
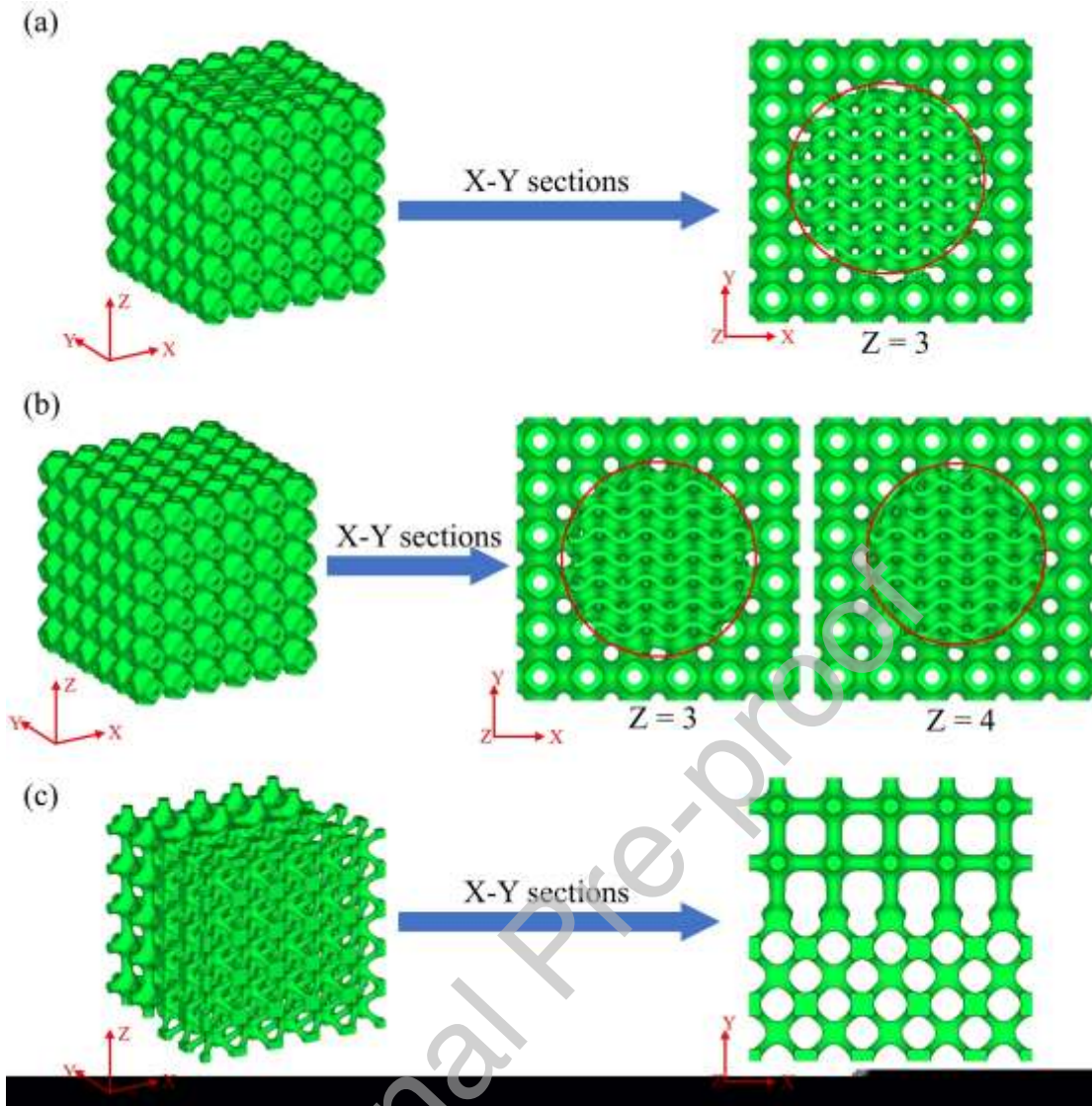
Fig. 13. Multi-morphology scaffolds: (a) Cylindrical boundary; (b) Spherical boundary; (c) Plane boundary along *y* axis.

5. Impact Overview and Conclusions

Owing to the vast number of TPMS applications, the generation of scaffold architectures for various applications is a highly studied topic. TPMS_Scaffold_Generator provides a free way to create many types of scaffold structures, which cover homogeneous architectures， functionally graded scaffold structures and multisymmetrical scaffolds. Therefore, their mechanical properties and other characteristics can be extensively researched. To better understand these scaffolds, an STL file created by TPMS_Scaffold_Generator can be obtained for finite-element analysis.

The generated STL documents can be used effectively to print 3D samples using a wide range of additive-manufacturing techniques. For example, we demonstrated the mechanical properties of

20

Ti$_6$Al$_4$V Fisher–Koch scaffolds. In addition, TPMS_Scaffold_Generator offers a new idea for multisymmetrical scaffolds, which can help researchers investigate crack initiation in TPMS scaffolds.

Declarations Conflict of Interest

The authors declare that they have no known competing financial interests or personal relationships that could appear to influence the work reported in this paper.

CRediT authorship contribution statement

Di Lin: Methodology, Investigation, Formal analysis, Software, Code, Writing – original draft, and Visualization. **Cong Zhang**: Writing – review & editing. **Xiyong Chen**: Writing – review & editing. **Nannan Wang**: Writing – review & editing. **Lei Yang**: Methodology, Writing – review & editing, Code, and Funding acquisition.

References

[1] Bhate D, Penick C A, Ferry L A, et al. Classification and selection of cellular materials in mechanical design: Engineering and biomimetic approaches. Designs 2019;3(1): 19.

[2] Alomar Z, Concli F. A review of the selective laser melting lattice structures and their numerical models. Advanced Engineering Materials 2020;22(12): 2000611.

[3] Zhang Q, Yang X, Li P, et al. Bioinspired engineering of honeycomb structure–Using nature to inspire human innovation. Progress in Materials Science 2015;74: 332-400.

[4] Ashb MFy. The properties of foams and lattices. Philosophical Transactions of the Royal Society A: Mathematical, Physical and Engineering Sciences 2006;364(1838): 15-30.

[5] Gibson L J. Cellular solids. Mrs Bulletin 2003;28(4): 270-274.

[6] Dong Z, Zhao X. Application of TPMS structure in bone regeneration. Engineered Regeneration 2021;2: 154-162. http://10.1016/j.engreg.2021.09.004.

[7] Al-Ketan O, Rowshan R, Al-Rub R K A. Topology-mechanical property relationship of 3D printed strut, skeletal, and sheet based periodic metallic cellular materials. Additive Manufacturing 2018;19: 167-183.

[8] Yan C, Hao L, Hussein A, et al. Evaluation of light-weight AlSi10Mg periodic cellular lattice structures fabricated via direct metal laser sintering. Journal of Materials Processing Technology 2014;214(4): 856-864.

[9] Torquato S, Donev A. Minimal surfaces and multifunctionality. Proceedings of the Royal Society of London. Series A: Mathematical, Physical and Engineering Sciences 2004;460(2047): 1849-1856.

[10] Abueidda DW, Jasiuk I, Sobh NA. Acoustic band gaps and elastic stiffness of PMMA cellular solids based on triply periodic minimal surfaces. Materials & design 2018;145: 20-27.

[11] Liverani E, Lutey A H, Fortunato A, et al. Characterization of lattice structures for additive manufacturing of lightweight mechanical components, International Manufacturing Science and Engineering Conference, American Society of Mechanical Engineers, 2017, 50732: V002T01A012.

[12] Li K, Chen W, Yin B, et al. A comparative study on WE43 magnesium alloy fabricated by laser powder bed fusion coupled with deep cryogenic treatment: Evolution in microstructure and mechanical properties. Additive Manufacturing 2023;77: 103814. http://10.1016/j.addma.2023.103814.

[13] Li K Ji, C, Bai S, et al. Selective laser melting of magnesium alloys: Necessity, formability, performance, optimization and applications. Journal of Materials Science & Technology 2023;154: 65-93. http://10.1016/j.jmst.2022.12.053.

[14] Thomas N, Sreedhar N, Al-Ketan O, et al. 3D printed spacers based on TPMS architectures for scaling control in membrane distillation. Journal of Membrane Science 2019;581: 38-49.

[15] Turner M D, Saba M, Zhang Q, et al. Miniature chiral beamsplitter based on gyroid photonic crystals. Nature Photonics 2013;7(10): 801-805.

[16] Kim J, Yoo D J. 3D printed compact heat exchangers with mathematically defined core structures. Journal of Computational Design and Engineering 2020;7(4): 527-550.

[17] Zhu L Y, Li L,Li Z A, et al. Design and biomechanical characteristics of porous meniscal implant structures using triply periodic minimal surfaces. Journal of Translational Medicine 2019;17(1): 1-10.

[18] O Al-Ketan, RK Abu Al-Rub. Multifunctional mechanical metamaterials based on triply periodic minimal surface lattices. Advanced Engineering Materials 2019;21(10): 1900524.

[19] Lee W. 'Cellular solids, structure and properties'. Materials Science and Technology 2000;16(2): 233.

[20] Yan X, Rao C, Lu L, et al. Strong 3D Printing by TPMS Injection. IEEE Trans Vis Comput Graph 2020;26(10): 3037-3050. http://10.1109/TVCG.2019.2914044.

[21] (2020) Netfabb lattice modules. [Online]: https://www.autodesk.co.uk/. https://www.autodesk.co.uk/.

[22] (2020) Materialise 3-matic. [Online]: https://www.materialise.com/en/industrial/software/structures. https://www.materialise.com/en/industrial/software/structures.

[23] (2020) nTopology. [Online]: https://ntopology.com/.

[24] (2020) Meshmixer. [Online]. Available: https://www.meshmixer.com/.

[25] I Maskery, L Parry, D Padrão, R Hague, I Ashcroft. FLatt Pack: A research-focussed lattice design program. Additive Manufacturing 2022;49(102510.

[26] Marten.(2021) STL Lattice Generator. [Online]. https://ww2.mathworks.cn/matlabcentral/fileexchange/48373-stl-lattice-generator.

[27] Hsieh M T,Valdevit L . Minisurf–A minimal surface generator for finite element modeling and additive manufacturing. Software Impacts 2020;6: 100026.

[28] Al-Ketan O, Abu Al-Rub R K. MSLattice: A free software for generating uniform and graded lattices based on triply periodic minimal surfaces. Material Design & Processing Communications 2021;3(6): e205.

[29] Afshar M, Anaraki AP, Montazerian H, et al. Additive manufacturing and mechanical characterization of graded porosity scaffolds designed based on triply periodic minimal surface architectures. J Mech Behav Biomed Mater 2016;62: 481-494. http://10.1016/j.jmbbm.2016.05.027.

[30] Rajagopalan S, Robb RA. Schwarz meets Schwann: design and fabrication of biomorphic and durataxic tissue engineering scaffolds. Med Image Anal 2006;10(5): 693-712. http://10.1016/j.media.2006.06.001.

[31] Schwarz HA. Gesammelte mathematische abhandlungen. American Mathematical Soc.1972.

[32] Michielsen K, Kole J. Photonic band gaps in materials with triply periodic surfaces and related tubular structures. Physical Review B 2003;68(11): 115107.

[33] Yoo D J. General 3D offsetting of a triangular net using an implicit function and the distance fields. International journal of Precision Engineering and Manufacturing 2009;10: 131-142.

[34] Wang S, Jiang Y, Hu J, et al. Efficient representation and optimization of TPMS-based porous structures for 3D heat dissipation. Computer-Aided Design 2022;142: 103123.

[35] Kapfer S C, Hyde ST, Mecke K, et al. Minimal surface scaffold designs for tissue engineering. Biomaterials 2011;32(29): 6875-82. http://10.1016/j.biomaterials.2011.06.012.

[36] Zhao M, Liu F, Fu G, et al. Improved mechanical properties and energy absorption of BCC lattice structures with triply periodic minimal surfaces fabricated by SLM. Materials 2018;11(12): 2411.

[37] Yang L, Mertens R, Ferrucci M, et al. Continuous graded Gyroid cellular structures fabricated by selective laser melting: Design, manufacturing and mechanical properties. Materials & Design 2019;162: 394-404. http://10.1016/j.matdes.2018.12.007.

[38] Fu J. Investigating the mechanical performance of the triply periodic minimal surface based metallic lattices made by micro laser powder bed fusion. Hong Kong: The Hong Kong Polytechnic University, 2022.

[39] Jones A, Leary M, Bateman S, et al. Parametric design and evaluation of TPMS-like cellular solids. Materials & Design 2022;221 :110908.

[40] Al-Ketan O, Rezgui R, Rowshan R, et al. Microarchitected stretching-dominated mechanical metamaterials with minimal surface topologies. Advanced Engineering Materials 2018;20(9): 1800029.

[41] Al-Ketan O, Rowshan R, Abu Al-Rub RK. Topology-mechanical property relationship of 3D printed strut, skeletal, and sheet based periodic metallic cellular materials. Additive Manufacturing 2018;19: 167-183. http://10.1016/j.addma.2017.12.006.

[42] Khoda AKM, Ozbolat IT, Koc B. Designing heterogeneous porous tissue scaffolds for additive manufacturing processes. Computer-Aided Design 2013;45(12): 1507-1523. http://10.1016/j.cad.2013.07.003.

[43] Yang N, Zhou K. Effective method for multi-scale gradient porous scaffold design and fabrication. Mater Sci Eng C Mater Biol Appl 2014;43: 502-5. http://10.1016/j.msec.2014.07.052.

[44] Li Y, Xia Q, Yoon S, et al. Simple and efficient volume merging method for triply periodic minimal structures. Computer Physics Communications 2021;264: 107956. http://10.1016/j.cpc.2021.107956.

[45] Yang N, Quan Z, Zhang D, et al. Multi-morphology transition hybridization CAD design of minimal surface porous structures for use in tissue engineering. Computer-Aided Design 2014;56: 11-21. http://10.1016/j.cad.2014.06.006.

[46] Yoo D J, Kim K H. An advanced multi-morphology porous scaffold design method using volumetric distance field and beta growth function. International Journal of Precision Engineering and Manufacturing 2015;16(9): 2021-2032. http://10.1007/s12541-015-0263-2.

[47] Liu C, Lertthanasarn J, Pham M S. The origin of the boundary strengthening in polycrystal-inspired architected materials. Nature Communications 2021;12(1): 4600. http://10.1038/s41467-021-24886-z.

[48] Zhang C, Qiao H, Yang L, et al. Vibration characteristics of additive manufactured IWP-type TPMS lattice structures. Composite Structures 2024;327: 117642. http://10.1016/j.compstruct.2023.117642.

[49] Jin J,Wu S , Yang L, et al. Ni–Ti multicell interlacing Gyroid lattice structures with ultra-high hyperelastic response fabricated by laser powder bed fusion. International Journal of Machine Tools and Manufacture 2023; 195: 10499. http://10.1016/j.ijmachtools.2023.104099.

Graphical Abstract
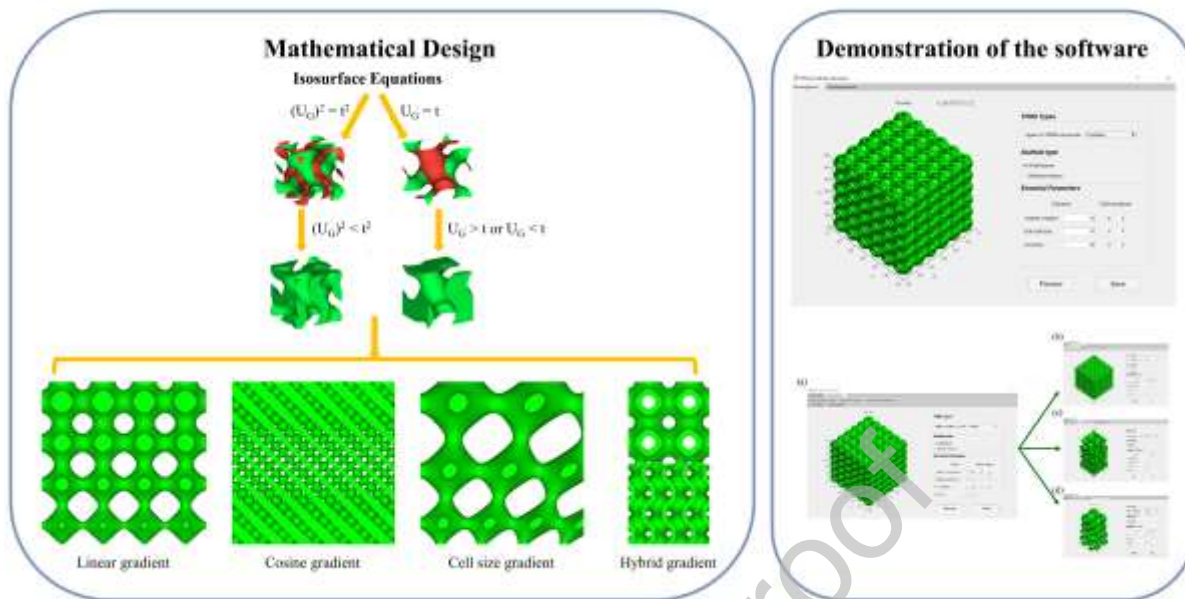
Declaration of Interest statement

The authors declare that they have no known competing financial interests or personal relationships that could have appeared to influence the work reported in this paper.